Journal of Catalysis **198,** 266–276 (2001)
doi:10.1006/jcat.2000.3110, available online at http://www.idealibrary.com on IDEAL®

CO Oxidation over Nonstoichiometric Nickel Manganite Spinels

C. Laberty,* C. Marquez-Alvarez,† C. Drouet,* P. Alphonse,* and C. Mirodatos†,[1]

*Laboratoire de Chimie des Matériaux Inorganiques, 118 route de Narbonne ESA 5070, 31062 Toulouse Cedex, France; and †Institut de Recherches sur la Catalyse, 2 Avenue Albert Einstein, 69626 Villeurbanne Cedex, France

Received August 11, 2000; revised October 24, 2000; accepted October 28, 2000; published online February 8, 2001

Nonstoichiometric nickel–manganese spinel oxides, $Ni_xMn_{3-x}\square_{3\delta/4}O_{4+\delta}$ ($1 \geq x \geq 0$), have been synthesized by calcination in air of mixed oxalates at 623 K. These materials are shown to be highly reactive for CO oxidation, some conversion being observed at room temperature for the most active solid ($x = 1.0$). The interaction of CO and O_2 with these oxides has been studied by *in situ* IR spectroscopy under steady-state and transient reaction conditions. A detailed mechanism is proposed wherein CO reacts with coordinatively unsaturated cations to give carbonyl complexes which in turn react with surface oxygen activated on anionic vacancies. Adsorbed and gaseous CO_2 also undergo much slower side reactions with lattice oxygen or surface hydroxide groups to give more stable hydrogen carbonate and carbonates species, which lead to catalyst deactivation. Marked effects of pretreatment are explained on the basis of the observed kinetics and the proposed mechanism.

Key Words: **nickel manganite; spinel; nonstoichiometry; catalytic CO oxidation; FTIR spectroscopy; DRIFT spectroscopy; reaction mechanism.**

INTRODUCTION

Nickel manganites are usually prepared by thermal decomposition of mixed manganese–nickel oxalate $Ni_{x/3}Mn_{(3-x)/3}C_2O_4 \cdot 2H_2O$ at 1173 K in air. These mixed oxides present a low specific surface area (ca. 1 $m^2\ g^{-1}$) and are stoichiometric (1, 2). In contrast, the thermal decomposition of manganese–nickel oxalate at low temperature ($T < 623$ K) recently investigated (3–5) gives cation-deficient spinels $Ni_xMn_{3-x}\square_{3\delta/4}O_{4+\delta}$. These oxides are finely divided materials, with their BET specific surface area larger than 100 $m^2\ g^{-1}$ and the average diameter of their crystallites about 10 nm (6).

Preliminary results indicated that these materials present a high reactivity toward molecules such as O_2, CO, or hydrocarbons, most likely due to their large nonstoichiometry and surface area. In order to investigate the potential use of such materials in environmental catalysis (such as CO post-combustion or CO oxidation for hydrogen purification), the present work reports a kinetic and IR investigation of CO oxidation over (a) nickel and manganese monometallic oxides and (b) mixed nickel–manganese spinels.

METHODS

Synthesis of oxide samples. Manganese and nickel monometallic oxides were prepared from thermal decomposition of manganese or nickel hydroxide, precipitated from a nitrate solution through addition of a solution of ammonium hydroxide. For transmission FTIR studies, about 50 mg of the required hydroxide was pressed (under a pressure of 5×10^8 Pa) to obtain 20-mm-diameter self-supported pellets. Mixed oxides $Ni_xMn_{3-x}\square_{3\delta/4}O_{4+\delta}$ were prepared by decomposition in air at 623 K for 6 h of mixed oxalates $Ni_{x/3}Mn_{(3-x)/3}(C_2O_4).2H_2O$ ($0 \leq x \leq 1$) obtained at room temperature by coprecipitation of an aqueous solution of nickel and manganese nitrates with a solution of ammonium oxalate. After 1 h, the mixture was filtered, washed several times with deionized water, and dried at 360 K in air. For transmission FTIR studies, about 100 mg of these oxides was pressed to obtain 20-mm-diameter self-supported pellets.

Catalytic activity. Catalytic tests were carried out in a tubular, fixed-bed flow reactor, at atmospheric pressure, in the temperature range 300–400 K, with a residence time $V/F = 0.01$ s and feeding reacting mixture $CO–O_2–N_2$ (1%–2%–97%). Reactants and products were analyzed by GC using two columns: 13× molecular sieve for N_2, O_2, and CO and Porapak Q for CO_2 separation. In order to account for the surface area, the intrinsic activity α (expressed in micromoles per second per square meter) was used to compare the tested samples.

In situ transmission Fourier transform infrared spectroscopy. Precursor or oxide pellets were placed in a stainless steel cell (Harrick, 45 mm total path length of the IR beam) connected to a conventional gas handling system. The sample could be heated or cooled in the range 240 to 700 K. Transmission FTIR spectra were recorded using a Nicolet 510 P spectrometer with a resolution of 4 cm^{-1}.

[1] To whom correspondence should be addressed. Fax: 04 72 44 53 99. E-mail: mirodato@catalyse.univ-lyon1.fr.

0021-9517/01 $35.00

In situ diffuse reflectance infrared Fourier transform spectroscopy. These experiments were carried out with a Spectra-Tech diffuse reflectance infrared cell (1.5 cm^3 of inner volume) fitted to a Nicolet 550 spectrometer. The cell was connected to the catalytic testing setup, in order to allow the gas mixtures to flow through the catalyst bed as for a conventional dynamic microreactor, to be further analyzed by GC and MS. About 50 mg of nickel manganite powder, sieved to 0.2–0.3 mm, was loaded into the cell. DRIFT spectra were recorded regularly (around 30 s acquisition time per spectrum with a resolution of 4 cm^{-1}) in order to observe the changes in the DRIFT pattern when temperature and gas composition were changed. The DRIFT spectra were converted into Kubelka–Munk units.

Surface area. Surface areas were measured by nitrogen adsorption (BET method) using a Micromeritics Flowsorb 2300.

X-ray diffraction. X-ray powder diffraction patterns were recorded using a Siemens diffractometer and Co$K\bar{\alpha}$ ($\lambda_{Co} = 0.17902$ nm) radiation.

RESULTS

Catalysts Characterization

Structure. XRD patterns (Fig. 1) of the $Ni_xMn_{3-x}\square_{3\delta/4}O_{4+\delta}$ samples show that these oxides are poorly crystallized. Dominant peaks in the XRD patterns correspond to the cubic spinel structure oxide. Lines of the X-ray pattern of the nickel-free compound ($x = 0$) can be indexed as tetragonal Mn_3O_4 (Hausmannite). Nickel oxide appears as an almost amorphous compound; only the main peaks of the cubic NiO phase can be identified.

Chemical composition. The nominal composition of the mixed oxides, determined by ionic chromatography, is reported in Table 1. However, rounded values will be used later for the sake of clarity.

Surface area. The BET surface area of the prepared $Ni_xMn_{3-x}\square_{3\delta/4}O_{4+\delta}$ oxides (Table 1) increases with the nickel amount by more than 1 order of magnitude, with respect to manganese oxide, up to $x = 0.8$. The pure nickel oxide displays, however, a relatively low surface (80 m^2/g).

TABLE 1

Composition, Surface Area, and Level of Nonstoichiometry δ of the Investigated Oxides

Chemical composition	S ($m^2 \cdot g^{-1}$)	δ
$Mn_3\square_{3\delta/4}O_{4+\delta}$	20	0.07 ± 0.01
$Ni_{0.29}Mn_{2.71}\square_{3\delta/4}O_{4+\delta}$	150	0.50 ± 0.05
$Ni_{0.45}Mn_{2.55}\square_{3\delta/4}O_{4+\delta}$	140	0.40 ± 0.03
$Ni_{0.71}Mn_{2.29}\square_{3\delta/4}O_{4+\delta}$	180	0.65 ± 0.05
$Ni_{0.84}Mn_{2.16}\square_{3\delta/4}O_{4+\delta}$	250	0.60 ± 0.03
$Ni_{1.04}Mn_{1.96}\square_{3\delta/4}O_{4+\delta}$	250	0.45 ± 0.03
$Ni\,\square_{\delta}O_{1+\delta}$	80	0.03 ± 0.01

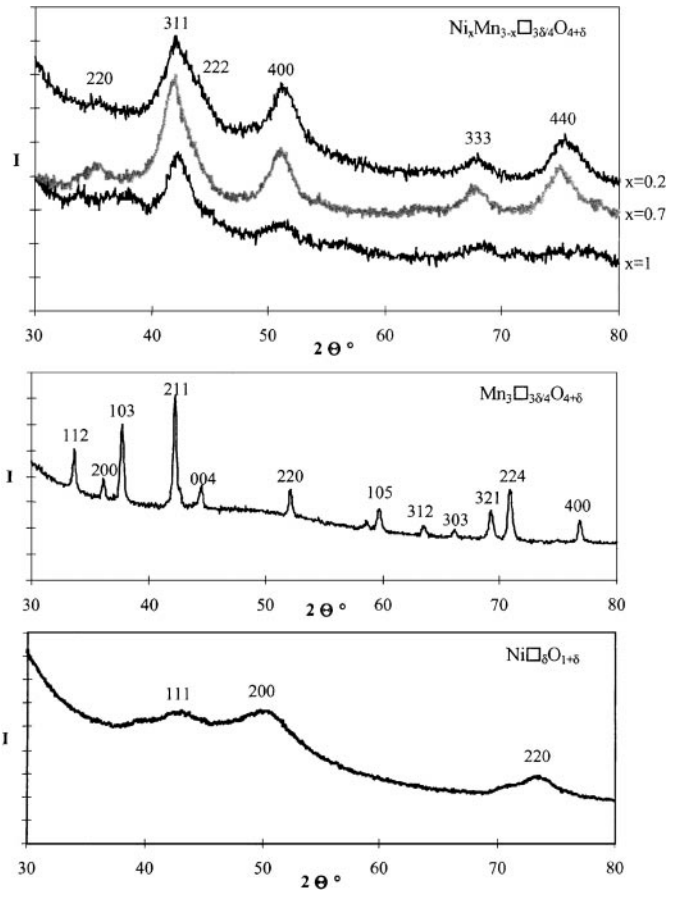

FIG. 1. XRD patterns of $Ni_xMn_{3-x}\square_{3\delta/4}O_{4+\delta}$, $Mn_3\square_{3\delta/4}O_{4+\delta}$, and $Ni\,\square_{\delta}O_{1+\delta}$ ($\lambda = 0.17902$ nm).

Level of nonstoichiometry. The nonstoichiometry of these oxides can be explained by the presence of cations with larger oxidation states than in stoichiometric oxides, implying the presence of cationic vacancies (3). For instance, Ni^{3+}, Mn^{3+}, and Mn^{4+} cations can be formed by oxidation of Ni^{2+}, Mn^{2+}, and Mn^{3+} cations, respectively, during the oxides' synthesis in air at low temperature. Upon heating in Ar, these nonstoichiometric oxides have been shown to lose part of their lattice oxygen in several steps tending to the stoichiometric formulas (7). The first release of oxygen, generally observed from 500 K (not observed with the Ni-free manganese oxide), might be assigned to the reduction of Ni^{3+} cations to Ni^{2+}, while the other ones (between 600 and 800 K) might correspond to the reduction of part of the Mn^{4+} and Mn^{3+} cations; additional experimental results are still required for unequivocal attribution of these steps. However, the total amount of released oxygen measured during temperature-programmed desorption (TPD)

experiments carried out in Ar allowed us to evaluate the nonstoichiometric level δ of the investigated oxides, which depends directly on the number of cationic vacancies per unit cell (Table 1). Though the monometallic oxides present some nonstoichiometric oxygen, approximately 10 times higher δ values are obtained with the mixed oxides, with a maximum corresponding to $x = 0.7$.

Cationic distribution. Since it has been found (8, 9) that surface ions in octahedral (Oh) configuration are more active than those in tetrahedral (Td) sites, the cationic distribution may be a worthwhile parameter to consider. Because of the strong preference of Ni^{2+} cations for Oh sites, stoichiometric nickel manganites are inverse spinels with the cationic arrangement $Mn^{2+}[Ni_x^{2+}Mn_x^{4+}Mn_{2-2x}^{3+}]O_4^{2-}$. Occupation of the Oh sites by Ni^{2+} induces the existence of $Mn^{3+/4+}$ redox couples on the same lattice sites. These couples lead to the high electrical conductivity of nickel manganites, while normal manganite spinels are all insulators. For $x = 1$, the cationic distribution would be $Mn^{2+}[Ni^{2+}Mn^{4+}]O_4^{2-}$. However, this arrangement does not account for the conductivity of this oxide, which implies that, for a high nickel content ($x > 0.7$), part of the Ni^{2+} cations must be in Td sites, giving the distribution $Ni_{(1-2\lambda)x}^{2+}Mn_{2\lambda x}^{2+}[Ni_{2\lambda x}^{2+}Mn_{2\lambda x}^{4+}Mn_{2-4\lambda x}^{3+}]O_4^{2-}$ where $0.25 \leq \lambda \leq 0.5$ depending on the nickel content and the thermal history of the sample (10). A previous WAXS study (11) has demonstrated that in cation-deficient nickel manganites, vacancies are mainly located in Td sites. As TPD profiles suggest the existence of Ni^{3+} in these oxides, their cationic distribution becomes quite complex. Among Ni^{3+}, Ni^{2+}, Mn^{3+}, and Mn^{4+}, Ni^{2+} has the lowest Oh site preference (12).

Catalytic Activity

Before the catalytic tests, the oxides were heated (for 1 h at 573 K) either in N_2 or in air; according to this pretreatment the catalysts were labeled prereduced (N_2) or preoxidized (air). For the most active oxides, the catalytic oxidation of CO already occurs at room temperature. Figure 2a shows that the intrinsic activity at 343 K increases regularly

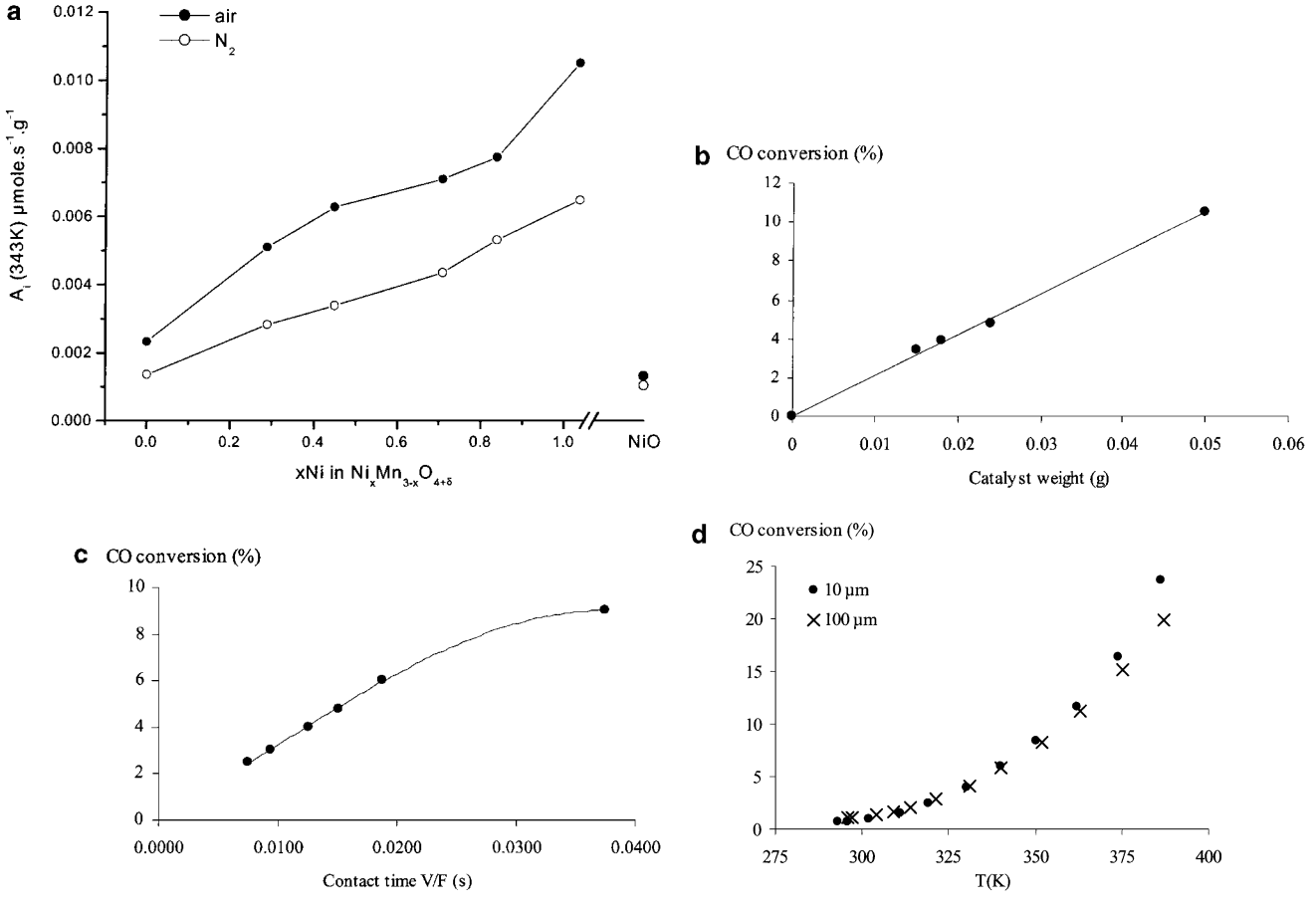

FIG. 2. (a) Changes in intrinsic activity A_i for CO oxidation at 343 K over nonstoichiometric oxides $Ni_xMn_{3-x}\square_{3\delta/4}O_{4+\delta}$, according to their nickel content (x_{Ni}) and pretreatment. Values for the pure NiO oxide are also reported for comparison. (b) Effect of catalyst weight on CO conversion at 343 K ($NiMn_2\square_{3\delta/4}O_{4+\delta}$; 343 K; $V/F = 0.015$ s). (c) Effect of contact time V/F on CO conversion at 343 K (0.025 g of $NiMn_2\square_{3\delta/4}O_{4+\delta}$). (d) Effect of particle size on CO conversion (0.025 g of $NiMn_2\square_{3\delta/4}O_{4+\delta}$; $V/F = 0.01$ s).

with nickel content (x) for the nonstoichiometric oxides, whatever the pretreatment. However, a much lower activity is found for the pure NiO oxide. In all cases, the preoxidized samples are more active than the prereduced ones.

From the Arrhenius plots giving straight lines with a very good correlation coefficient ($r^2 \geq 0.999$), constant activation energies values were determined over the whole range of temperature (300–400 K) when CO conversion was varied from less than 0.1% to more than 10% (Table 2). It can be noted that rather similar E_a values are found for all the mixed oxides for any nickel content and pretreatment, while slightly higher values correspond to the monometallic oxides.

The possible occurrence of either external or internal mass transfer limitations was discarded after checking the following points: (i) under the applied experimental conditions (conversion below 10%) the CO conversion was found to increase linearly with the catalyst weight and the contact time (up to $V/F = 0.02$) (Figs. 2b and 2c, respectively); (ii) the conversion (below 10%) was found to be independent of particle size between 10 and 100 μm (Fig. 2d).

For all the oxides, the reaction order with respect to O_2 was found close to zero. The order with respect to CO was found in the range 0.5 to 0.6 for the mixed oxides and equal to 0.9 for the pure nickel oxide.

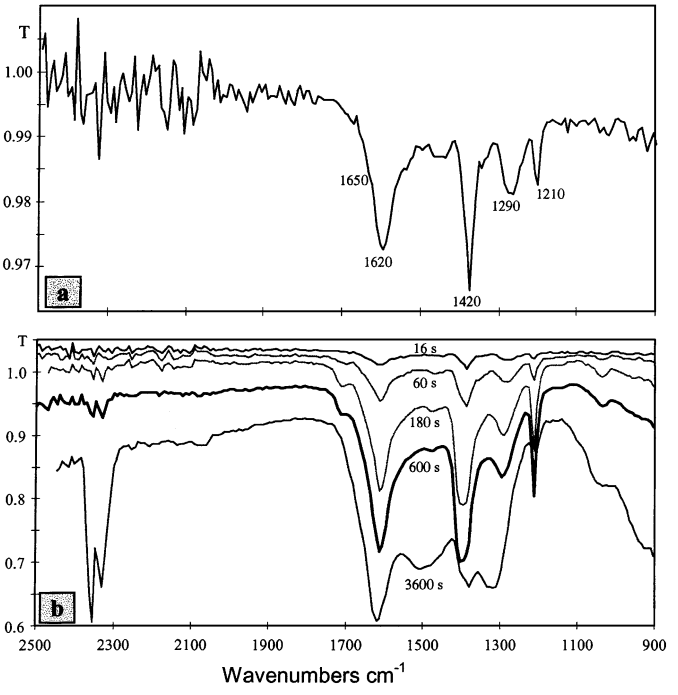

FIG. 3. FTIR spectra of outgassed $Mn_3\square_{3\delta/4}O_{4+\delta}$ under CO (10^3 Pa) at 253 K. (a) 16 s after CO admission. (b) Changes with time. Spectra are offset for clarity.

IR Transmission Study

A. Manganese oxide. The $Mn(OH)_2$ pellet was outgassed for several hours at room temperature, until a residual pressure of 5×10^{-4} Pa was attained; the temperature was then slowly raised to the decomposition temperature (573 K) and kept at this value for 24 h.

Static CO and CO_2 adsorption on outgassed surface. Figure 3 shows selected IR spectra of the manganese oxide sample as a function of time under CO (10^3 Pa) at 253 K. The spectrum recorded 16 s after CO admission (Fig. 3a) shows several bands in the range 1100–1700 cm^{-1}, characteristic of carbonate species (14, 15). For larger contact times, the number and intensity of these bands increase and two absorption bands develop after 180 s in the range 2300–2400 cm^{-1} (Fig. 3b), that become prominent after 1 h. In the last spectrum, these two bands show the characteristic fine structure envelope of branches P (2360 cm^{-1}) and R (2340 cm^{-1}) of the rotation–vibration band of the gaseous CO_2 asymmetric stretching vibration (mode ν_3 at 2349 cm^{-1}). At shorter contact times, the presence of another weak band at ca. 2340 cm^{-1} can be inferred since the intensity ratio of these two P and R bands, which is 1.2 for pure gaseous CO_2, is found to be lower than 1, then to increase progressively to about 1.2 with time on stream. This means that the R branch of the gaseous CO_2 ν_3 rotation–vibration band overlaps this other band at 2340 cm^{-1}. This band, that seems to develop in the first few minutes, can tentatively be assigned to the ν_3 vibration mode of adsorbed CO_2. The small band shift with respect to the free CO_2 pure vibrational transition (2349 cm^{-1}) would indicate some weak interaction of the CO_2 molecule with the oxide surface.

Upon outgassing at room temperature, 1 min is required to remove completely the CO_2 gas. This resistance to outgassing may be explained by a trapping effect of CO_2 species in the sample meso-micropores, as already suggested in (13). In contrast, although the intensity of the bands in the range 1100–1700 cm^{-1} is significantly lowered, the carbonate species are still observed even after 24 h under vacuum.

From the numerous works published on adsorbed carbonate species (14, 15), the main bands of the previous spectra can be assigned to the three following species:

—Hydrogen carbonate, resulting from the interaction of CO_2 with surface hydroxyl groups: 1210 cm^{-1} (OH bending), 1420 cm^{-1} (symmetric stretching), and 1620 cm^{-1} (asymmetric stretching). It can be noticed that these species are the first to be removed upon outgassing, along with CO_2.

—Bidentate carbonate: 980 cm^{-1} (symmetric stretching), 1300 cm^{-1} (asymmetric stretching), and 1650 cm^{-1} (C=O stretching).

—Monodentate carbonate: ca. 1380 cm^{-1} (symmetric stretching) and ca. 1500 cm^{-1} (asymmetric stretching). These bands appear simultaneously with those of the adsorbed CO_2 (after about 3 min of contact).

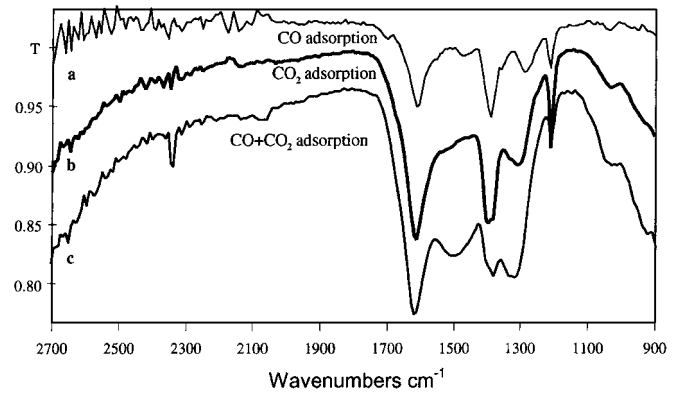

FIG. 4. FTIR spectra of outgassed $Mn_3\square_{3\delta/4}O_{4+\delta}$, 16 s after contact with 10^3 Pa of CO (a), CO_2 (b), and $CO + CO_2$, 1:1 molar ratio (c), at 253 K. Spectra are offset for clarity.

When the manganese oxide is directly contacted with gaseous CO_2 (10^3 Pa) at 253 K (Fig. 4b), not only the formation of hydrogen and bidentate carbonates is confirmed after 16 s, but also the formation of monodentate carbonates (1380 and 1500 cm^{-1}). It is amazing that practically no bands of adsorbed CO_2 appear on the spectrum (Fig. 4b). This means that most of the gaseous CO_2 reacts (i) with the surface hydroxyl groups to give hydrogen carbonate, and (ii) with the coordinatively unsaturated sites to give bidentate or monodentate carbonate. In contrast, when CO and CO_2 are coadsorbed, the band at 2340 cm^{-1}, assigned to weakly adsorbed CO_2, is formed; surface saturation is attested by the strong increase of the bands assigned to monodentate carbonate species (1380 and 1500 cm^{-1}).

Interaction with a flowing stoichiometric mixture $CO + 1/2O_2$. Figure 5 shows the change of the IR spectrum with time on $CO\ (2\%) + O_2\ (1\%) + N_2$ (balance) stream at 253 K for the manganese oxide sample, initially outgassed. Though these spectra are similar to the spectrum observed for the static adsorption of CO (Fig. 3), several differences can be pointed out:

(i) A weak CO stretching vibration–rotation doublet band (P and R branches) due to gaseous CO is observed showing maxima at ca. 2115 and 2173 cm^{-1}.

(ii) The first spectrum (recorded at 16 s) already shows bands corresponding to monodentate carbonate species (1380 and 1500 cm^{-1}), as well as adsorbed and gaseous CO_2 (2340–2360 cm^{-1}).

(iii) Absorption bands of hydrogen carbonates (1200 and 1400 cm^{-1}) strongly decrease in the spectra recorded after 30 min on stream.

B. Nickel oxide. The $Ni(OH)_2$ wafer was outgassed for several hours at room temperature until a residual pressure of 5×10^{-4} Pa was reached, and then the temperature was slowly raised to the decomposition temperature (473 K) and kept at this value for 24 h. A strong absorption is observed in the range 1200–1500 cm^{-1} after this treatment, most likely due to bulk carbonates formation during the preparation of the hydroxide pellet (at variance with the manganese oxide which is outgassed at higher temperature (573 K)).

Static CO adsorption on outgassed surface. After contact of the sample with CO (10^3 Pa) at 253 K (Fig. 6) infrared bands corresponding to adsorbed and gaseous CO_2 develop (2300–2400 cm^{-1}). In contrast with manganese oxide (Fig. 3a), these bands appear from the first spectrum recorded after 16 s. In the range 2000–2300 cm^{-1} several bands are present in the first spectrum but their intensity rapidly decreases and they vanish after less than 1 min. These bands may be assigned to carbonyl-like species resulting from the interaction of CO with coordinatively unsaturated Ni cations. In the literature, ν_{CO} frequencies reported for CO adsorption on nickel-containing compounds are 2050–2110 cm^{-1} for Ni^0–CO complexes, 2135–2140 cm^{-1} for Ni^+–CO, and 2190–2200 cm^{-1} for Ni^{2+}–CO (16). However, although it is likely that the strongest band at 2200 cm^{-1} corresponds to the interaction of CO with a single Ni^{2+} cation, the lower frequency bands could result from the transient formation of polycarbonyl species (two

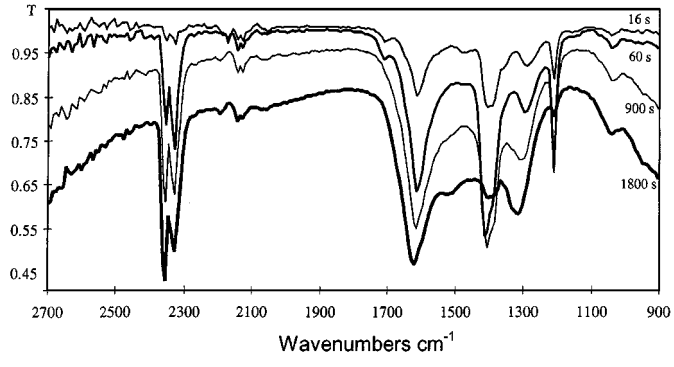

FIG. 5. Changes with time of FTIR spectra recorded on outgassed $Mn_3\square_{3\delta/4}O_{4+\delta}$ under a flowing gas mixture, $CO\ (2\%) + O_2\ (1\%) + N_2$ (balance), at 253 K. Spectra are offset for clarity.

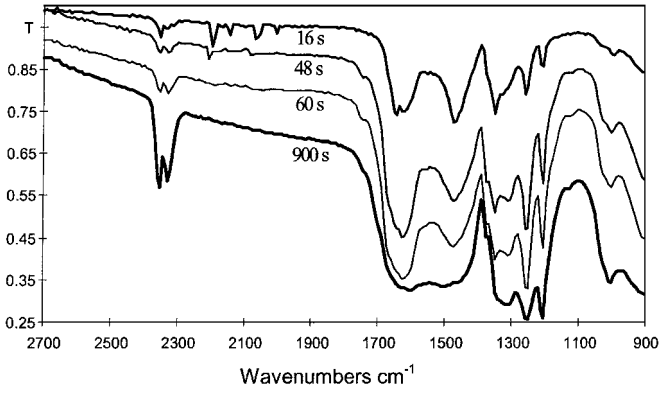

FIG. 6. Changes with time of FTIR spectra recorded on outgassed $Ni\square_\delta O_{1+\delta}$ under CO (10^3 Pa) at 253 K. Spectra are offset for clarity.

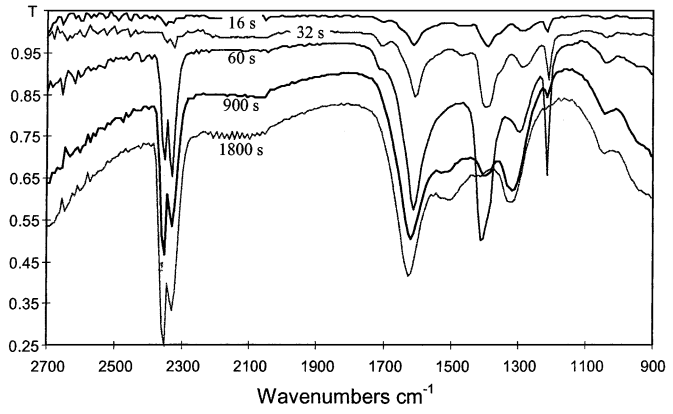

FIG. 7. Changes with time of FTIR spectra recorded on a preoxidized surface of $Ni\square_{\delta}O_{1+\delta}$ under CO (10^3 Pa) at 253 K. Spectra are offset for clarity.

or three CO molecules interacting with the same nickel cation) (13).

In the range 1100–1700 cm^{-1} the bands characteristic of carbonate species develop rapidly and to a much larger extent than for the manganese oxide. These bands then become so large that they are no longer resolved. The main bands of the first spectrum (16 s) are rather similar to those observed with the manganese oxide, indicating the presence of the same species: hydrogen carbonate and mono- and bidentate carbonates.

Static CO adsorption on preoxidized surface. Figure 7 shows the spectra recorded after contact with CO (10^3 Pa) at 253 K on the NiO sample pretreated with O_2 (2×10^4 Pa). In this case, no carbonyl species are formed, indicating the absence of coordinatively unsaturated Ni cations after preadsorption of O_2. In the region 900–1700 cm^{-1}, less numerous bands are observed with a lower overall intensity than on an outgassed surface. The main bands (1210, 1410, and 1620 cm^{-1}) can be attributed to hydrogen carbonate; after 15 min these bands strongly decrease and new bands at 1325 and 1510 cm^{-1} replace them. The disappearance of hydrogen carbonate corresponds to a production of gaseous CO_2 as evidenced by the large increase in the intensity of bands at 2360–2340 cm^{-1}. Hence, hydrogen carbonates seem to be less stable species; they decompose to give gaseous CO_2 and are replaced by mono- and bidentate carbonates. Probably part of the monodentate species comes from the readsorption of the gaseous CO_2. The comparison between Figs. 7 and 6 shows that the preadsorption of O_2 on an oxide surface reduces severely the number and type of formed carbonates species.

Static adsorption of a stoichiometric mixture CO + 1/2O_2. When the initially outgassed nickel oxide is contacted at 253 K with a mixture of CO (2%) + O_2 (1%) + N_2 (balance), spectra similar to those recorded after static adsorption of CO (Fig. 6) are observed in the range 900–1900 cm^{-1}; however, no carbonyl species are detected in the range 2000–2300 cm^{-1}.

C. Nickel manganites. Before adsorption experiments, the wafer of mixed oxide is outgassed for 1 h at 573 K under vacuum (10^{-4} Pa).

Static CO adsorption on an outgassed surface. Figure 8 shows the spectra recorded on a $NiMn_2\square_{3\delta/4}O_{4+\delta}$ outgassed sample after contact with CO (10^3 Pa) at 253 K. Two strong and sharp bands are observed in the high-frequency range. The first one, at 2340 cm^{-1}, corresponds to weakly adsorbed CO_2 and is rather stable with time. The second band, at 2187 cm^{-1}, can be unequivocally assigned to the carbonyl-like species resulting from the interaction between CO and metallic cations. These species are far more stable than those observed with the nickel oxide since they decrease only after 600 s.

In the low-frequency range, the formation of mono- and bidentate carbonate and hydrogen carbonate species is attested by the bands at 1030, 1210, 1290, and 1410 cm^{-1} as well as by the broad band centered at 1605 cm^{-1}. These bands slightly increase with time without formation of new bands. The weak bands at 1800 cm^{-1}, observed only in this case, cannot be assigned to carbonyl species; they could correspond to organic carbonates (14).

By comparing these spectra and those recorded on a monometallic oxide of manganese (Fig. 3a) and nickel (Fig. 6) it can be pointed out that, at variance with manganese and nickel oxides, a large amount of adsorbed CO_2 and carbonyl species is rapidly formed. The formation of carbonate species is also observed but to a lower extent than on the nickel oxide. Though decreasing with time, the carbonyl bands remain far more stable than those observed with the nickel oxide: even after 30 min, formation of CO_2 gas is not detected. Hence, strong interactions exist between CO_2 and the surface of these mixed oxides.

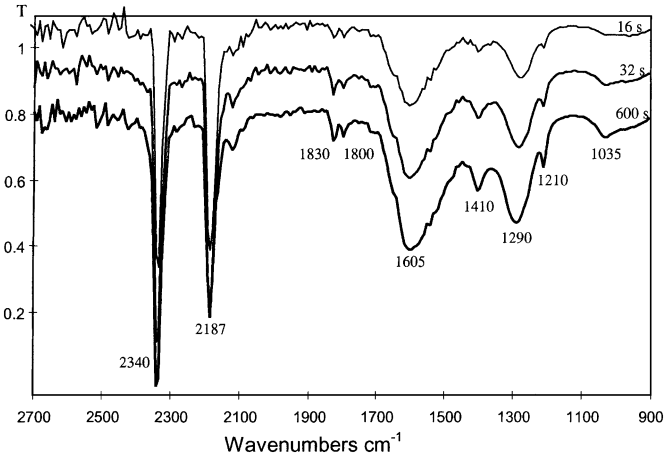

FIG. 8. Changes with time of FTIR spectra recorded on outgassed $NiMn_2\square_{3\delta/4}O_{4+\delta}$ under CO (10^3 Pa) at 253 K. Spectra are offset for clarity.

By comparing spectra recorded after 16 s on several mixed oxides with different Ni/Mn ratios, very few differences are observed except for the carbonyl bands. On $NiMn_2\square_{3\delta/4}O_{4+\delta}$ only one symmetrical absorption band is observed at 2187 cm^{-1} while for $Ni_{0.8}Mn_{2.2}\square_{3\delta/4}O_{4+\delta}$ and $Ni_{0.7}Mn_{2.4}\square_{3\delta/4}O_{4+\delta}$ two bands can be identified at 2165 and 2187 cm^{-1}. Although carbonyl bands do not develop during the CO adsorption on the pure manganese oxide, it has been shown (17) that, at low temperature (<150 K), adsorption of CO on spinel manganese oxide could lead to the formation of carbonyl species with Mn cations. Hence, the band at 2187 cm^{-1} could be assigned to carbonyl complexes, either with Ni^{2+} or Mn^{3+} cations in fourfold coordination or with Mn^{4+} cations in fivefold coordination, the band at 2165 cm^{-1} being attributed to complexes with Mn^{3+} cations in fivefold coordination.

Upon outgassing at room temperature, the band assigned to adsorbed CO_2 is completely removed within 1 min, and the hydrogen carbonate bands (1620, 1410, and 1210 cm^{-1}) decrease much more rapidly than the monodentate carbonate bands (1500 and 1380 cm^{-1}); the complete removal of carbonate species is obtained after 24 h of outgassing.

Static CO adsorption on preoxidized surface. As observed on nickel oxide, preadsorption of oxygen (2×10^4 Pa) produces a drastic decrease in the surface reactivity of the $NiMn_2\square_{3\delta/4}O_{4+\delta}$ sample. After 16 s of contact with CO (10^3 Pa) at 253 K, only weak bands of carbonates are observed, which slowly increase. Hydrogen carbonates (1220, 1400, and 1620 cm^{-1}) are more easily formed on an oxidized than on an outgassed surface. It takes more than 30 min to observe weak CO_2 bands. Again, no carbonyl species are formed because of the absence of coordinatively unsaturated cations after preadsorption of O_2. Therefore, it can be stated that the formation of adsorbed CO_2 is related to the occurrence of carbonyl species but not of carbonate species.

Static adsorption of stoichiometric mixture $CO + 1/2O_2$. Figure 9 shows the spectra of a $NiMn_2\square_{3\delta/4}O_{4+\delta}$ sample, initially outgassed, contacted at 253 K with a gas mixture of

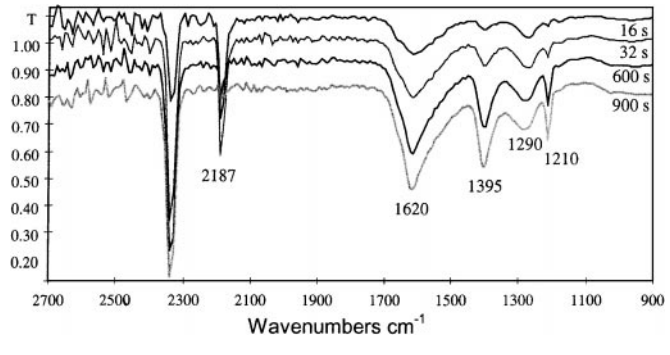

FIG. 9. Changes with time of FTIR spectra recorded on outgassed $NiMn_2\square_{3\delta/4}O_{4+\delta}$ under a mixture, CO (2%) + O_2 (1%) + N_2 (balance), total pressure 10^5 Pa, at 253 K. Spectra are offset for clarity.

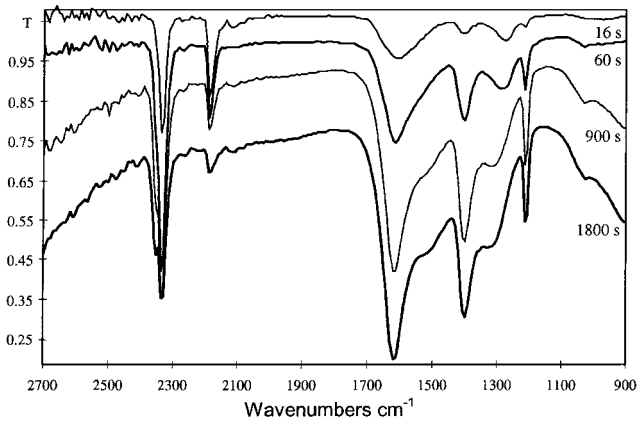

FIG. 10. Changes with time of spectra recorded on outgassed $NiMn_2\square_{3\delta/4}O_{4+\delta}$ under a flowing gas mixture, CO (2%) + O_2 (1%) + N_2 (balance), at 253 K. Spectra are offset for clarity.

CO (2%) + O_2 (1%) + N_2 (balance). Although the spectra are similar to those recorded during static adsorption of CO on an outgassed surface (Fig. 8), some differences can be observed:

(i) In the presence of oxygen, the bidentate carbonate bands (1025, 1290, and 1650 cm^{-1}) are less intense, while the hydrogen carbonate bands (1210, 1395, and 1620 cm^{-1}) exhibit an increased intensity.

(ii) The overall intensity of carbonate bands in the region 1100–1700 cm^{-1} is not significantly modified by the presence of oxygen, whereas the maximum intensity of the carbonyl band (2187 cm^{-1}) decreases by 40%. Actually the carbonyl absorption appears to be related to the CO/O_2 ratio in the gas mixture: when this ratio becomes lower than 2 (nonstoichiometric by excess of O_2) carbonyl species are no longer formed.

Interaction with a flowing stoichiometric mixture $CO + 1/2O_2$. Under dynamic conditions (flowing CO (2%) + O_2 (1%) + N_2 (balance) gas mixture at 253 K) the first spectrum recorded after 16 s over the $NiMn_2\square_{3\delta/4}O_{4+\delta}$ sample (Fig. 10) is rather similar to the one obtained for static adsorption (Fig. 9). However, the following differences are noted for longer time on stream:

(i) While in the static experiment only the band at 2340 cm^{-1} (assigned to adsorbed CO_2) is observed in the region 2300–2400 cm^{-1}, after 900 s under flow the presence of gaseous CO_2 is evidenced by the development of its asymmetric stretching rotation–vibration band, observed as a shoulder at 2360 cm^{-1}, which intensity increases with time on stream.

(ii) As soon as gaseous CO_2 is formed, the concentration of monodentate carbonate species increases, suggesting that gaseous CO_2 is readsorbed.

(iii) The intensity of the carbonyl band (2187 cm^{-1}) decreases more slowly; this band is still observed after 1800 s.

Transient DRIFT Study

A transient DRIFT study has been carried out on the $NiMn_2\square_{3\delta/4}O_{4+\delta}$ oxide in order to determine the CO oxidation mechanism. Before analysis, the sample was heated at 573 K for 1 h either under helium flow (prereduced) or under O_2 (20%)/He (80%) flow (preoxidized).

Step transient from He to CO/He flowing mixture. Figure 11 reports some of the DRIFT spectra recorded on the preoxidized $NiMn_2\square_{3\delta/4}O_{4+\delta}$ sample, after switching at 293 K from flowing He to CO (1%) + Ar (tracer) + He (balance). The spectra show the bands assigned to carbonate species (1700–1200 cm^{-1}), adsorbed CO_2 (2340 cm^{-1}), and carbonyl (2187 cm^{-1}). Additionally, Fig. 11 shows the presence of rotation–vibration bands corresponding to gaseous CO (2100–2200 cm^{-1}) and CO_2 (2300–2400 cm^{-1}) in the whole series of spectra. However, both doublet bands are partly overlapped by the adsorbed CO_2 (2340 cm^{-1}) and CO (2187 cm^{-1}) bands.

Similar bands are observed in the IR spectra of the prereduced sample, although hydrogen carbonate bands show lower intensity. The normalized changes in band intensity with time on stream are depicted in Fig. 12 (symbols) together with the changes in outlet gas composition, as determined by online MS analysis (lines). Both gaseous and adsorbed CO_2 are formed in the first seconds after the switch (accounting for the gas hold-up delay) superimposed with the inert Ar tracer response. The concentration of both species reaches a steady-state level after ca. 100 s. The delay between the Ar and the CO responses indicates that part of the admitted CO is irreversibly adsorbed and/or converted to CO_2. This is confirmed by the transient formation of both adsorbed (2340 cm^{-1}, square symbols) and gaseous CO_2 (dashed line from MS analysis), slightly delayed after the CO (adsorbed and gaseous) curves. A residual pseudo-steady-state production of CO_2 is attained after ca. 800 s.

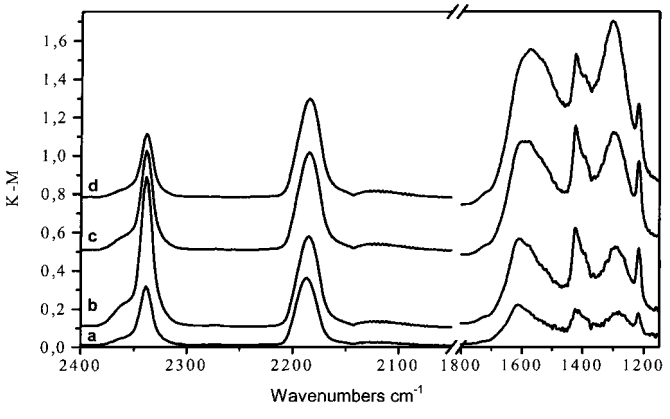

FIG. 11. DRIFT spectra recorded on preoxidized $NiMn_2\square_{3\delta/4}O_{4+\delta}$ under CO (1%) + Ar (tracer) + He (balance) flow at 293 K for (a) 13 s, (b) 77 s, (c) 258 s, and (d) 909 s. The spectrum of the sample under He flow has been subtracted. Spectra are offset for clarity.

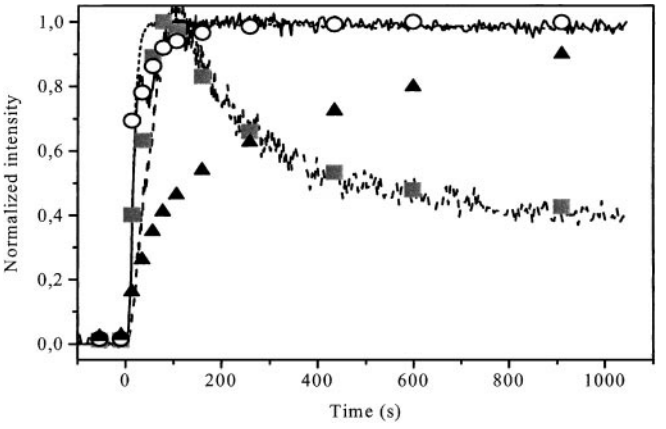

FIG. 12. Step change from He to CO (1%) + Ar (tracer) + He (balance) flow on preoxidized $NiMn_2\square_{3\delta/4}O_{4+\delta}$ at 293 K in the DRIFT cell. Changes with time of the normalized MS intensity for CO (full line), CO_2 (dashed line), and Ar (dotted line) in the gas phase, and normalized intensity of IR bands of adsorbed CO (2187 cm^{-1}, circles), CO_2 (2340 cm^{-1}, squares), and carbonates (1200 to 1700 cm^{-1}, triangles).

Though this production could be partly due to oxygen traces present in the flowing CO/He mixture, it indicates that there are also rather stable adspecies on the surface slowly decomposing into gaseous CO_2. The latter can most likely be related to the accumulation/decomposition of carbonate species observed in the DRIFT spectra. As a matter of fact, by integrating the whole absorption range of carbonate species (1200–1700 cm^{-1}), the transient curve with triangles shown in Fig. 12 is obtained. The shape of the curve clearly demonstrates that the formation of carbonates is much slower than that of CO and CO_2 adspecies, their concentration still increasing after 800 s. A more accurate analysis reveals actually that during a first period up to ca. 100 s, i.e., up to the maximum of CO_2 production, there is an increase of the bands at 1610, 1420, 1280, and 1220 cm^{-1} (corresponding to hydrogen carbonates). Later on, when the CO_2 production decreases and stabilizes, the large bands at 1525 and 1320 cm^{-1}, which correspond to mono- and bidentate carbonates, develop continuously. This trend which was already outlined in the transmission study confirms that hydrogen carbonate species are formed prior to carbonate, the latter invading progressively the catalytic surface.

For the reverse transient experiment (shift from CO/He to He), CO and CO_2 gas and adspecies disappear very rapidly while the carbonate/hydrogen carbonate bands decrease slowly and only to a limited extent (a few percent of the previously attained intensity).

Step transient from He to stoichiometric $CO + 1/2O_2$ gas mixture. The DRIFT spectra recorded on the $NiMn_2\square_{3\delta/4}O_{4+\delta}$ sample after switching at 293 K from flowing He to the CO (2%) + O_2 (1%) + He (balance) gas mixture are similar to those recorded during the previous transient study in the absence of O_2 but with a marked increase

in band intensity. The concentration of CO_2 in the outlet gas flow reaches rapidly a steady-state value corresponding to the previously reported catalytic activity measured in a fixed-bed microreactor, confirming that the catalytic oxidation of CO to CO_2 undoubtedly occurs at room temperature on these oxides.

DISCUSSION

A preliminary approach of the reaction mechanism for the catalytic CO oxidation on these nonstoichiometric oxides can be discussed on the basis of the above results.

The apparent activation energy (Table 2) and the reaction orders are found to be only slightly dependent on the catalyst composition for the mixed oxides. Therefore, the reaction mechanism is probably the same for all these materials. It could however be slightly different for the pure oxides. Since the possible occurrence of any mass transfer limitation has been discarded for most of the applied reaction conditions, the overall process has to be considered as catalytically controlled.

The reaction order with respect to O_2 is found to be close to zero and CO_2 can be produced even without O_2 (at least during a transient period). This means that the CO oxidation on these oxides proceeds with surface or bulk oxygen. In this respect, the gaseous oxygen dissociation required for producing/regenerating these adsorbed oxygen species can be considered as a fast process. In contrast, a noninteger partial order was found with respect to CO pressure ($n_{CO} = 0.5$–0.6). Such a value suggests that the CO oxidation could proceed both via a direct reaction of gaseous CO with adsorbed oxygen ($n_{CO} = 1, n_{O_2} = 0$, i.e., an Eley–Rideal mechanism) and via a surface reaction between adsorbed CO and adsorbed O ($n_{CO} = 0$, $n_{O_2} = 0$, i.e., a Langmuir–Hinshelwood mechanism). An inhibiting effect of CO adsorption on oxygen adsorption due to a competitive adsorption process could also be considered to explain the experimental values of n_{CO}: the apparent order would result from the combination of a positive value due to the CO pressure effect and a negative one due to the accumulation of adsorbed CO inhibiting O_2 activation. In this respect, for the case of catalysts where CO adsorption is not favored (such as on NiO pure oxide), one should have logically a more positive order, as experimentally observed ($n_{CO} = 0.9$).

TABLE 2

Apparent Activation Energies of Monometallic and Mixed Oxides for CO Oxidation at 323 K

	x						
	0	0.3	0.5	0.7	0.8	1	NiO
E_a (kJ · mol^{-1}), Preoxidized catalysts	45 ± 5	36 ± 2	36 ± 2	35 ± 3	32 ± 2	30 ± 3	40 ± 5
E_a (kJ · mol^{-1}), Prereduced catalysts	55 ± 5	40 ± 2	40 ± 2	39 ± 2	36 ± 2	36 ± 2	55 ± 5

In order to get more details on these possible catalytic routes, the main properties of the various adspecies (carbonyl, adsorbed CO_2, carbonates, and hydrogen carbonates) observed by *in situ* infrared spectroscopy (transmission and diffuse reflectance) under reaction conditions can be analyzed, focusing on their accumulation and stability.

Carbonyl Species

These species are essentially observed after CO adsorption on the prereduced mixed oxides as a unique and intense band at 2187 cm^{-1} and are assigned unambiguously to monocarbonyl CO–M^{n+}. M may be either coordinatively unsaturated Mn or Ni cations. The formation of these carbonyl species is however strongly hindered after oxygen preadsorption or in the case of coadsorption of CO and O_2 with a low CO/O_2 ratio. For the case of NiO, much less numerous and less stable carbonyl species are observed and, in addition, the observation of several bands suggests polycarbonyls species (Ni–CO_n). Thus on NiO, there is a much lower surface concentration of adsorbed CO (since they are unstable and gathered as polycarbonyl). They are not detected under reaction conditions in the presence of oxygen.

These statements strongly suggest that the carbonyl species which are accumulated as monocarbonyl on the most active solids (mixed oxides) participate in the reaction, but via complex routes possibly including an inhibiting effect for oxygen adsorption.

Adsorbed CO_2

These adspecies are observed at 2340 cm^{-1} under reacting atmosphere (carbon monoxide without or with oxygen) on all samples but (i) they are much more abundant and more stable on mixed oxides than on pure oxides, and (ii) they are in all cases more abundant in the presence of oxygen. In the absence of oxygen, they are observed essentially during a transient period which corresponds to the production of gaseous CO_2 (Fig. 12). Therefore, this form of adsorbed CO_2 also belongs to the catalytic process. Since adsorbed CO_2 is accumulating essentially on the mixed oxides with a large surface area, a plausible assumption would be to consider them as weakly adsorbed species retained in the meso-/micropores of the solid (nickel manganite particles are 10-μm-size clusters of 5–10-nm-size crystallites).

Hydrogen Carbonates and Mono- and Bidentate Carbonates

These species are identified in the IR range 1100–1700 cm^{-1}. As a general trend, the hydrogen carbonate

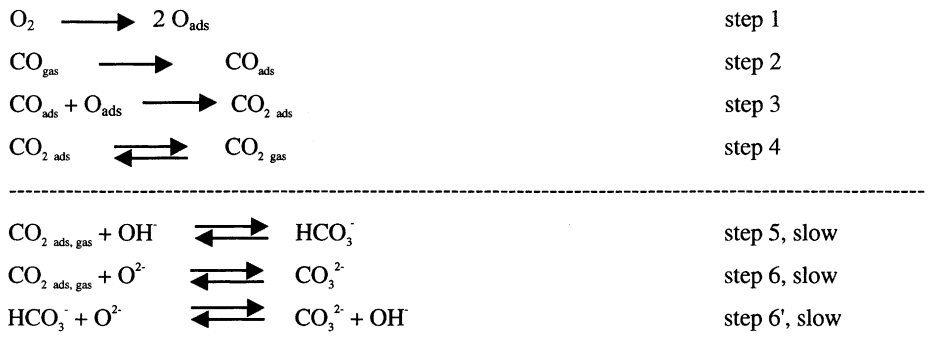

SCHEME 1. Sequential elementary steps occurring during the CO oxidation process.

species HCO_3^-, which derives from the reaction of acidic CO_2 molecules with basic OH^- hydroxyl groups, are found to form rapidly when adsorbed and gaseous CO_2 is produced and are easily removed upon outgassing (together with adsorbed and gaseous CO_2). In contrast, the carbonate species (mono- and bidentate CO_3^{2-}) which derive from the interaction of CO_2 with basic O^{2-} lattice oxygen atoms are formed after and at the expense of the hydrogen carbonate species. They progressively accumulate on the catalyst and are only partly and slowly decomposed upon outgassing. Their accumulation may lead to some catalyst deactivation, but seems little dependent on oxygen partial pressure. This is expected from the fact that the lattice O^{2-}, required for carbonate formation, is not affected by oxygen adsorption, at variance with the lattice vacancies.

Catalytic Routes

On the basis of the above analyses of surface occupancy under reaction conditions (in the presence or in the absence of oxygen), and from the transient DRIFT experiments showing the fast adsorption of CO as surface carbonyls followed after some delay by the transient formation of both adsorbed and gaseous CO_2, and further on by the formation of hydrogen carbonate and finally of carbonates, a tentative scheme for CO oxidation can be proposed as in Scheme 1.

In Scheme 1, gaseous oxygen dissociates rapidly into adsorbed species (step 1). Gaseous carbon monoxide also accumulates rapidly and competitively on the surface (step 2). The latter in turn reacts with the former to form weakly adsorbed CO_2 (step 3), in equilibrium with gaseous CO_2 (step 4). For the case of pure nickel oxide where the accumulation of surface carbonyl (step 2) is not favored, steps 2 and 3 merge into a single step.

In a much slower side process, therefore not participating directly in the main catalytic cycle (steps 1–4), gaseous or adsorbed CO_2 may also interact with surface hydroxyls and with lattice oxygen atoms to give hydrogen carbonate and carbonate species, respectively (steps 5 and 6). The consecutive decomposition of hydrogen carbonates into carbonates is also tentatively represented by step 6′. With time on stream, the latter species accumulate, limiting the adsorption of the less stable carbonyl species, which leads to catalyst deactivation.

Indeed this tentative mechanistic scheme based on surface analysis should be strengthened by a complete kinetic study leading to a robust kinetic model from which the actual RDS would be derived (under progress).

Catalytic Sites

The nature of each catalytic site involved in Scheme 1 can now be discussed in more detail. The formation of adsorbed CO in step 2 has been shown to involve coordinatively unsaturated cations (CUS) which may be either manganese or nickel cations. The by far largest concentration observed on the mixed oxides and the very small concentration observed on the pure manganese oxide favor the hypothesis that CO is principally coordinated to CUS nickel cations in the spinel structure; however, the larger specific surface area of mixed oxides also implies a larger concentration of lattice defects and hence of adsorption sites. The surface step 3 involves both adsorbed CO and surface oxygen species. The clear relationship between intrinsic activity and nickel concentration for the mixed oxides (Fig. 2) strongly supports this catalytic role of surface carbonyl for these materials. With regard to adsorbed oxygen species, the most active materials, i.e., the mixed oxides, were also found to display the highest level of nonstoichiometry (Table 1). This parameter, evaluated from released oxygen during TPD experiments, tends to include several types of nonstoichiometric oxygen species, related to redox couples of cations such as Ni^{3+}/Ni^{2+} or Mn^{4+}/Mn^{3+}. Whatever the exact nature of the involved process and cation, the relationship between nonstoichiometry and catalytic activity can be explained by assuming that the active oxygen able to react with adsorbed CO derives from the fast dissociative activation of gaseous oxygen on pair sites—anionic vacancies/reduced cation—as often proposed in oxidation processes (18),

$$2[M^{n+} + \square] + O_2 \rightarrow 2[O^- + M^{(n+1)+}], \qquad [1]$$

possibly via intermediates such as O_2^- peroxide anion. For the Ni-containing mixed oxides, M could either be Ni with $n=2$ or Mn with $n=3$. Thus, step 3 can be written as a surface reaction between monocarbonyl and electrophilic oxygen adspecies O^- as

$$Ni^{2+}-CO+[O^-+M^{(n+1)+}] \rightarrow CO_{2\ ads}+Ni^{2+}+M^{n+}+\square. \quad [2]$$

As already mentioned, the direct reaction of gaseous CO with O^- adspecies could be considered as the boundary case of the above process, when CO accumulation is not favored like for NiO.

This scheme also assumes a competitive adsorption between CO and O_2 on CUS cations which explains why carbonyl complexes are no longer formed for an O_2/CO concentration ratio larger than the stoichiometry.

For the slow secondary reaction of CO_2 with basic sites leading to hydrogen carbonate and carbonates (steps 5 and 6), surface OH groups and lattice O^{2-} atoms are the obvious active sites. The stable species which are progressively accumulating (especially the carbonate ones) would hinder the above redox processes possibly through the bidentate carbonate formation which may consume surface vacancies as follows:

$$CO_2 + O^{2-} + \square \rightarrow \quad [3]$$

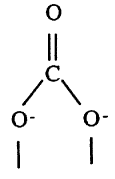

A quantitative evaluation of the active sites for step 3, i.e., the surface vacancies associated with oxidizable cation $[M^{n+}+\square]$, can be attempted by measuring the transient amount of CO_2 produced under flowing CO in the absence of oxygen. By integrating the CO_2 transient response obtained for the prereduced mixed oxide $NiMn_2\square_{3\delta/4}O_{4+\delta}$ in Fig. 12 (without considering the background production due to both oxygen traces in the feed and the slow decomposition of accumulated carbonates) or for the preoxidized sample, we find that about 5% and 1% of the amount of surface Ni and Mn cations would be involved in the redox equations [1] and [2] for the preoxidized and prereduced samples, respectively. These values indicate that only a small fraction of the mixed oxide cations participate in the oxygen activation and CO oxidation steps, as expected from the nonstoichiometric level and the calculated cation distributions. In addition, the state of the catalytic surface is clearly shown to depend strongly upon the solid pretreatment, as checked experimentally throughout the present study.

CONCLUSION

Calcination in air of mixed oxalates at 623 K gives nonstoichiometric nickel–manganese spinel oxides. These materials are very active catalysts for CO oxidation since conversion is already observed at room temperature. The intrinsic catalytic activity of these mixed oxides increases with the nickel content.

Based on a thorough IR analysis of the adspecies formed under steady-state and transient reaction conditions, a mechanism is proposed which assumes a surface reaction between adsorbed carbonyl species (most likely on Ni^{2+} cations) and electrophilic oxygen species (O^- type) arising from the reaction of gaseous oxygen with surface vacancies. Side processes of CO_2 readsorption and accumulation over basic OH^- and O^{2-} ions, into hydrogen carbonate and carbonate respectively, are also considered and their participation to the catalyst deactivation is demonstrated. This complex mechanism involving redox cationic couples and nonstoichiometric oxygen species may explain the unusually high activity of the mixed oxides as compared to the much less active pure manganese or nickel oxides.

REFERENCES

1. Jabry, E., Boissier, G., Rousset, A., Carnet, R., and Lagrange, A., *J. Phys. Colloq., C1* **47**, 843 (1986).
2. Gillot, B., Baudour, J. L., Bouree, F., Metz, R., Legros, R., and Rousset, A., *Solid State Ionics* **58**, 155 (1992).
3. Tang, X. X., Manthiram, A., and Goodenough, J. B., *J. Less-Common Met.* **156**, 357 (1989).
4. Feltz, A., and Topfer, J., *Z. Anorg. Allg. Chem.* **576**, 71 (1989).
5. Topfer, J., and Jung, J., *Thermochim. Acta* **202**, 281 (1992).
6. Laberty, C., Alphonse, P., Demai, J. J., Sarda, C., and Rousset, A., *Mater. Res. Bull.* **32**(2), 249 (1996).
7. Drouet, C., Alphonse, P., and Rousset, A., *Solid State Ionics* **123**, 25 (1999).
8. Cimino, A., and Schiavello, M., *J. Catal.* **20**, 202 (1971).
9. Yao, H. C., and Shelef, M., *J. Phys. Chem.* **78**, 2490 (1974).
10. Fritsch, S., Legros, R., and Rousset, A., in "Ceramics: Charting the future" (P. Vincenzini, Ed.), Advances in Science and Technology 2D, p. 2565, Techna Sr, Paris, 1995.
11. Laberty, C., Verelst, M., Lecante, P., Alphonse, P., Mosset, A., and Rousset, A., *J. Solid State Chem.* **129**, 271 (1997).
12. Navrotsky, A., and Kleppa, O. J., *J. Inorg. Nucl. Chem.* **29**, 2701 (1967).
13. Gugliminotti, E., Cerruti, L., and Borello, E., *Gazz. Chim. Ital.* **107**, 503 (1977).
14. Little, L. H., "Infrared spectra of adsorbed species." Academic Press, London, 1966.
15. Davydov, A. A., "Infrared spectroscopy of adsorbed species on the surface of transition metal oxides." Wiley, New York, 1990.
16. Lokhov, Y., and Davydov, A. A., *Kinet. Katal.* **21**, 1523 (1980).
17. Angevaare, P. A. J. M., Aarden, J. R. S., Linn, J. R., Zuur, A. P., and Ponec, V., *J. Electron Spectrosc. Relat. Phenom.* **54/55**, 795 (1990).
18. Bielanski, A., and Haber, J., "Oxygen in Catalysis." Marcel Dekker, New York, 1991.